NANO LETTERS

2009
Vol. 9, No. 1
449-452

Hybrid Solar Cells from P3HT and Silicon Nanocrystals

Chin-Yi Liu, Zachary C. Holman, and Uwe R. Kortshagen*

Department of Mechanical Engineering, University of Minnesota, 111 Church Street SE, Minneapolis, Minnesota 55455

Received November 12, 2008; Revised Manuscript Received December 16, 2008

ABSTRACT

We are reporting new hybrid solar cells based on blends of silicon nanocrystals (Si NCs) and poly-3(hexylthiophene) (P3HT) polymer in which a percolating network of the nanocrystals acts as the electron-conducting phase. The properties of composite Si NCs/P3HT devices made by spin-coating Si NCs and P3HT from a common solvent were studied as a function of Si NC size and Si NC/P3HT ratio. The open-circuit voltage and short-circuit current are observed to depend on the Si NC size due to changes in the bandgap and surface-area-to-volume ratio. Under simulated one-sun A.M. 1.5 direct illumination (100 mW/cm^2), devices made with 35 wt % Si NCs 3−5 nm in size showed 1.15% power conversion efficiency.

Hybrid solar cells based on mixtures of conjugated polymers and inorganic semiconductor nanocrystals are attractive because they may combine the desirable properties of both materials. Conjugated polymers are solution-processable and have strong visible absorption so that only thin films are required in solar cells. As a result, they have great potential for inexpensive large-scale solar cell manufacturing. Semiconductor nanocrystals have properties which differ from those in the bulk due to quantum confinement. It is therefore possible to tune the absorption spectra of nanocrystals by changing their size. Nanocrystals may be blended with polymers without compromising the solution-based fabrication process, and a percolated network of nanocrystals in hybrid devices may provide high-mobility pathways for carriers.

Various promising hybrid solar cells have been reported, including devices which utilize polymer in conjunction with cadmium selenide (CdSe),[1] zinc oxide (ZnO),[2] titanium dioxide (TiO_2),[3] lead sulfide (PbS),[4] lead selenide (PbSe),[5] and copper indium disulfide ($CuInS_2$)[6] spherical nanocrystals; CdSe nanorods;[7] and CdSe hyperbranched nanocrystals.[8] These devices were made by spin-coating nanocrystal/polymer blends onto substrates where they phase segregate at the nanometer length scale to facilitate exciton dissociation and subsequent charge carrier transport. In these hybrid solar cells the organic semiconductor usually acts as the hole-transport medium while the inorganic nanocrystals take the role of electron-transporting medium. CdSe nanocrystals/poly(3-hexylthiophene) (P3HT) solar cells currently hold the efficiency record for hybrid devices, with power conversion efficiencies (PCEs) greater than 2%. ZnO nanocrystals/poly(2-methoxy-5-(2′-ethyl)hexyloxy-1,4-phenylenevinylene) (MEH-PPV) and TiO_2 nanocrystals/P3HT solar cells have also shown impressive efficiencies,[2,3] but their performance is likely limited by the poor visible absorption of the wide-band-gap nanocrystals. Hybrid solar cells made with PbS, PbSe, and $CuInS_2$ nanocrystals have not yet shown promising efficiencies.

Silicon (Si) has enjoyed years of success in the solar cell and microelectronics industries and is a prime candidate for polymer−nanocrystal solar cells given its abundance, nontoxicity, and strong UV absorption. Gowrishankar et al. have fabricated hybrid bilayer cells consisting of either P3HT or MEH-PPV spun onto hydrogenated amorphous silicon (a-Si:H) and achieved efficiencies of 0.16%.[9] Adikaari et al. have improved on this result by nanostructuring and crystallizing the a-Si:H to increase interfacial area and carrier mobility.[10] They reported a best efficiency of 0.87%, although the fill factor of 0.23 of the device was low. Here, we employ blends of free-standing silicon nanocrystals (Si NCs) and regioregular P3HT to form nanocrystal−polymer hybrid solar cells. As shown in Figure 1a, the band alignment of Si and P3HT is such that exciton dissociation at the interface is energetically favorable even for bulk Si (dashed lines) and becomes increasingly favorable for quantum-confined Si NCs (solid lines). These devices also have the potential for enhanced exciton dissociation compared to the aforementioned Si-containing hybrid devices due to the greater interfacial area afforded by the blend architecture. Additionally, Si NCs may contribute to the light absorption in these devices, offering an advantage over previous hybrids using wide-band-gap semiconductor nanocrystals. In order to

* Corresponding author, uk@me.umn.edu.

10.1021/nl8034338 CCC: $40.75
Published on Web 12/29/2008

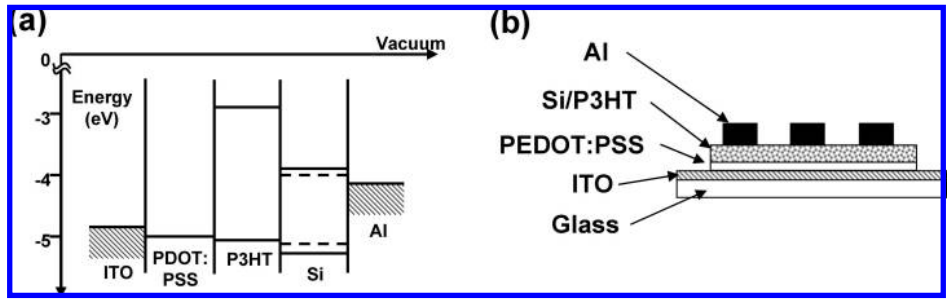

Figure 1. (a) Energy band diagram of a Si NCs/P3HT solar cell. The dotted lines represent the valence and conduction bands of bulk Si, while the solid lines are representative of 4 nm Si NCs. (b) Schematic of a Si NCs/P3HT hybrid solar cell. Thin films of PEDOT:PSS and Si NCs/P3HT were spun sequentially on transparent ITO substrates. Aluminum metal electrodes (100 nm thick) were deposited on the top.

optimize solar cell performance, different Si NC sizes and Si NC/P3HT ratios were explored.

Silicon nanocrystals were synthesized in a nonthermal radio frequency (rf) plasma via dissociation of silane and collected on mesh filters.[11] By variation of chamber pressure, precursor flow rate, and rf power, Si NCs can be made with average sizes between 2 and 20 nm. To minimize oxidation, Si NC collection and handling were conducted in a nitrogen-purged glovebag and Schlenk line. As-produced Si NCs were dispersed in 1,2-dichlorobenzene (DCB, ACROS) and sonicated to form a cloudy solution. Prior to film formation, Si NCs were characterized by transmission electron microscopy (TEM), Fourier-transform infrared spectroscopy (FTIR), and X-ray diffraction (XRD). TEM, which was used to determine average size, shows spherical particles with narrow size distributions (standard deviation <25% of the mean size, see Figure S1 in the Supporting Information). Three groups of Si NCs were used in this study: Si NCs that were 3−5 nm in diameter, 5−9 nm in diameter, and 10−20 nm in diameter. FTIR spectra of all Si NCs show Si−H_x bands (Supporting Information, Figure S2a), indicating that the nanocrystal surfaces are terminated by hydrogen. It should be noted that hydrogen passivation does not provide sufficient steric stabilization to overcome interparticle van der Waals attractions and prevent agglomeration of the Si NCs in solution. However, van der Waals attractions can be significantly reduced by choosing a solvent with a Hamaker constant comparable to the Si NC Hamaker constant.[12] We have observed that Si NCs are more stable in DCB than other common solvents such as toluene or hexane and flocculate slowly over the course of weeks, not hours. We believe that this occurs because the dielectric constant of Si (11.7) is much closer to that of DCB (9.8) than toluene (2.4) or hexane (1.9).[13] XRD patterns for all sizes of particles display the (111), (220), (311), (400), and (331) diffraction peaks of diamond cubic Si (Supporting Information, Figure S2b).

Solar cells were fabricated by spin-coating Si NCs/P3HT onto indium tin oxide (ITO) coated glass substrates. ITO-coated substrates (25 mm × 20 mm) of 8−12 Ω/square resistance (Delta Technologies, LTD) were first patterned using photolithography and etched in a mixture of hydrochloric acid, nitric acid, and water. This left two 2.3 mm wide ITO strips near the middle of the glass substrate. The

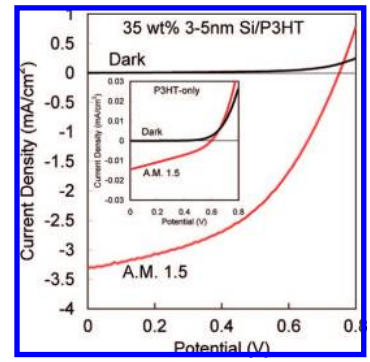

Figure 2. Current−voltage characteristic ($I-V$) of a 35 wt % 3−5 nm Si NCs/P3HT solar cell (main window) and P3HT-only solar cell (inset). The $I-V$ characteristic of the hybrid device was recorded under 100 mW/cm^2 A.M. 1.5 direct conditions and shows 1.15% PCE and a fill factor of 0.46 with 3.3 mA/cm^2 short-circuit current density and 0.75 V open-circuit voltage. The current densities of the P3HT-only device are roughly 2 orders of magnitude smaller than that for the hybrid device.

patterned ITO substrates were cleaned with acetone, isopropanol, and distilled water and treated with an oxygen plasma for 10 min to clean the substrate surface and make it hydrophilic.[14] Roughly 50 nm of poly(3,4- ethylenedioxythiophene)/poly(styrenesulfonate) (PDOT:PSS) (H. C. Starck) was spun onto the oxygen-plasma-treated ITO substrates. Excess water was then removed from the PDOT:PSS film by baking at 130 °C for 5 min. P3HT (Rieke Metals, Inc.) was dissolved in a DCB solution which contained a known quantity of Si NCs. The Si NCs/P3HT solution was then sonicated a second time and spun on top of the PDOT:PSS layer in a glovebox to form a film approximately 100 nm thick. Finally, 2 mm wide aluminum (Al) electrodes (100 nm thick) were evaporated on top of the Si NCs/P3HT film to complete the thin film solar cells. A schematic in Figure 1b illustrates the device configuration. The active area of each device is 0.046 cm^2.

Figure 2 shows current−voltage ($I-V$) characteristics of typical Si NCs/P3HT (main figure) and P3HT-only (inset) devices both in the dark and under A.M. 1.5 direct solar irradiation. For all devices—which were illuminated through the ITO side—diode behavior was seen in the dark and in the light. Predictably, P3HT-only devices exhibit little photoactivity since the lack of an electron-accepting material means any built-in potential must arise from the junctions

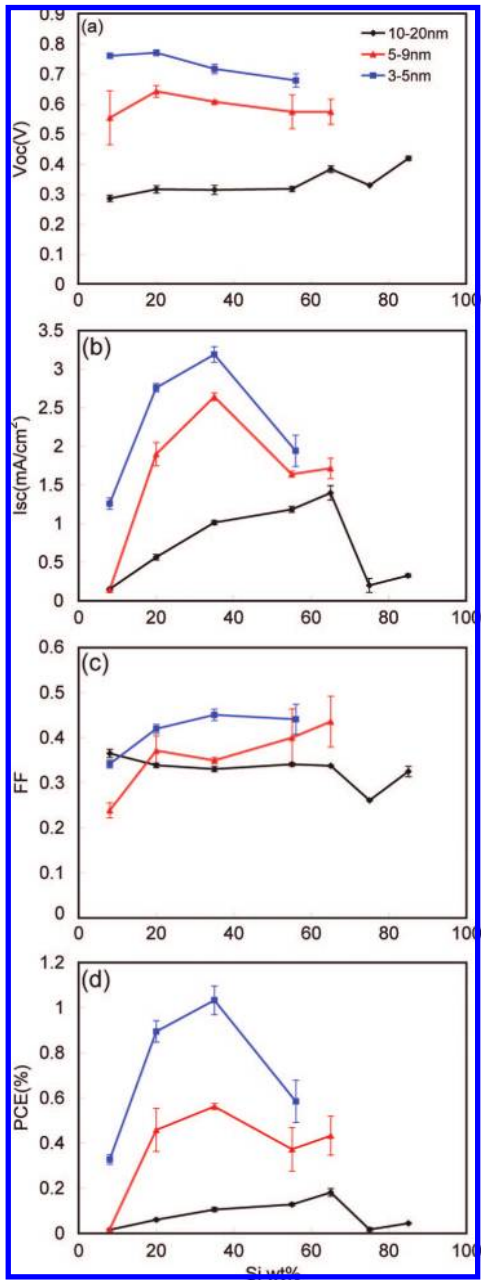

Figure 3. Silicon NCs/P3HT solar cell performance characteristics for devices with different Si NCs/P3HT ratios and NC sizes. 3−5, 5−9, and 10−20 nm Si NCs are represented with blue squares, red triangles, and black diamonds, respectively. Each data point and associated error bar represent an average value and standard deviation from a set of six devices on one substrate. Defective devices, which comprise less than 10% of all devices, are ignored.

with the electrodes. By contrast, devices in which Si NCs are included have shown PCEs above 1.1%.

To understand the role of the Si NCs in these solar cells, device performance was studied as a function of Si NCs/P3HT ratio for each of the three Si NC size groups (Figure 3). Figure 3a indicates that the open-circuit voltage (V_{oc}) is inversely related to NC size, regardless of the materials ratio. This dependence clearly indicates that the Si NCs play an active role in exciton dissociation. We believe the inverse trend is due to a widening of the Si NC bandgap, which can be observed in the blue shift of the photoluminescence for sizes below about 10 nm.[11] An opening of the Si NC bandgap results in a smaller conduction band offset between the Si NCs and P3HT (Figure 1a), resulting in less voltage lost during exciton dissociation.

Short-circuit current (I_{sc}) also increases with decreasing Si NC size (Figure 3b). This result is surprising. Fewer interparticle hopping events should be required to transport an electron to the Al electrode in devices with larger Si NCs, enhancing electron transport. A corresponding increase in I_{sc} is not observed, suggesting that electron transport through the Si NCs is not the limiting factor in the devices. Instead, the current could be limited by a bottleneck in the hole transport material, P3HT, or the efficiency of exciton dissociation could decrease rapidly with increasing Si NC size. Assuming a mobility of 10^{-3} cm^2/(V s) and a device thickness of 100 nm, the diffusion time of holes in P3HT is on the order of 1 μs. Transport in P3HT may be limiting I_{sc} if this time is comparable to or longer than the trapping or recombination times. It is also probable that exciton dissociation is enhanced in devices with smaller Si NCs due to their greater surface-area-to-volume ratio and wider band gap, and this may play a role in the observed trend in I_{sc}.

For all Si NC sizes, I_{sc} peaks when the Si NCs/P3HT weight ratio is between 30 and 70%. This likely occurs because a balance between electron and hole transport material must be struck and the interfacial area between them maximized. However, film morphology also plays a role. Scanning electron microscopy (SEM) was performed on Si NCs/P3HT films spun onto gold-coated Si wafer chips which were used to avoid sample charging. SEM image analysis shows films that are 100−200 nm thick on average but that have nonuniform distributions of Si NCs and therefore nonhomogeneous surfaces (Figure S3 of the Supporting Information). For high Si NC concentrations, Si NC agglomeration seriously deteriorates film uniformity and is expected to decrease I_{sc} because of increased film resistance. Solar cells with Si NCs/P3HT weight ratios greater than 55% for 3−5 nm Si NCs and 65% for 5−9 nm Si NCs could not be fabricated because the solution viscosity increased until spin-coating a macroscopically uniform film is no longer feasible.

The measured fill factor was nearly independent of Si NC size and the Si NCs/P3HT ratio (Figure 3c). As a result, the calculated PCEs follow the trends observed in V_{oc} and I_{sc}, and are shown in Figure 3d. It should be noted that these results are reproducible, with greater than 90% yield rate of functional devices. The best solar cell performance was obtained for 35 wt % Si NCs that were 3−5 nm in diameter. This cell had a 1.15% PCE and a fill factor of 0.46, with I_{sc} of 3.3 mA/cm^2 and V_{oc} of 0.75 V.

The incident photon-to-current conversion efficiency (IPCE) for the 35 wt % 3−5 nm device is shown in Figure 4. The device is most efficient near 500 nm, where the IPCE is 26%. In order to understand the spectral dependence observed in the IPCE, the optical absorption spectra of P3HT only, Si NCs only, and Si NCs/P3HT films on quartz substrates were measured and are displayed in Figure 5. P3HT has a strong

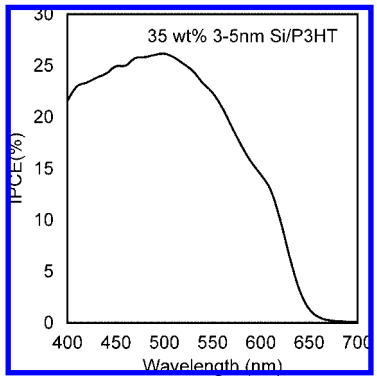

Figure 4. Incident photon-to-current efficiency spectrum of a 35 wt % 3−5 nm Si NCs/P3HT solar cell.

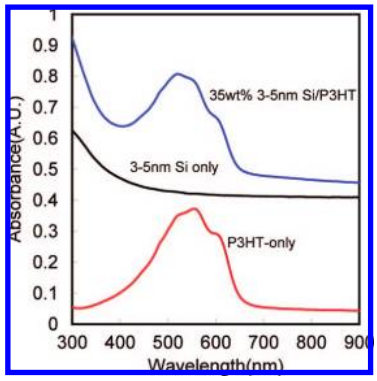

Figure 5. Room-temperature optical absorption spectra of P3HT, Si NCs, and 35 wt % 3−5 nm Si NCs/P3HT films on quartz. The absorbance of the Si NCs/P3HT film below 400 nm is due to Si NCs.

absorption band between 450 and 650 nm. Silicon nanocrystals have little absorption in the visible compared to P3HT, with the absorption coefficient of bulk Si only one-tenth of that of P3HT at 500 nm.[15,16] However, Si NCs absorb strongly in the UV, complementing the absorption of P3HT. In the P3HT-only film, the maximum absorption is located at 560 nm, but the Si NCs/P3HT film peaks at 520 nm due to the additional absorption by Si NCs. Comparing the absorption spectra with the IPCE spectrum in Figure 4, we see that most of the collected current results from P3HT absorption, although Si NC absorption appears to boost the IPCE below 500 nm.

In summary, we have demonstrated Si NCs/P3HT solar cells fabricated by spin-coating blends of Si NCs and P3HT onto ITO-coated glass substrates. An optimatization of Si NC size and Si NCs/P3HT ratio showed that small Si NC sizes and roughly 35 wt % Si NCs produced the best devices, with efficiencies as high as 1.15%. Both open-circuit voltage and short-circuit current improved with decreasing size, suggesting that larger interfacial area and nanocrystal band-gap aid device performance. In these devices, visible light absorption and exciton generation in P3HT is the primary source of photocurrent, and Si NCs only contribute to current generation in the UV. Nonuniform film morphologies were observed in SEM due to Si NC agglomeration, and this is expected to reduce device efficiency. Despite this limitation, our device performance indicates that Si NCs are a good candidate for future organic−inorganic hybrid solar cells, especially given the lack of toxicity and elemental abundance of Si.

Acknowledgment. This work was primarily supported by the MRSEC program of NSF (DMR-0212302). We also acknowledge partial support by the NSF NIRT program (CTS-0506672) and the Minnesota Initiative for Renewable Energy and the Environment (IREE, LG-C5-2005). We utilized the University of Minnesota Characterization Facility which receives partial support from the NSF under the NNIN program. Z.C.H. was supported by the IGERT program of the NSF (DGE-0114372).

Supporting Information Available: Si NC synthesis details, TEM and SEM images, and FTIR and XRD spectra. This information is available free of charge via the Internet at http://pubs.acs.org.

References

(1) Greenham, N. C.; Peng, X.; Alivisatos, A. P. *Phys. Rev. B* **1996**, *54*, 17628.
(2) Beek, W. J. E.; Wienk, M. M.; Janssen, R. A. J. *Adv. Funct. Mater.* **2006**, *16*, 1112.
(3) Kwong, C. Y.; Choy, W. C. H.; Djurišiić, A. B.; Chui, P. C.; Cheng, K. W.; Chan, W. K. *Nanotechnology* **2004**, *15*, 1156.
(4) Günesa, S.; Fritz, K. P.; Neugebauer, H.; Sariciftci, N. S.; Kumar, S.; Scholes, G. D. *Sol. Energy Mater. Sol. Cells* **2007**, *91*, 420.
(5) Cui, D.; Xu, J.; Zhu, T.; Paradee, G.; Ashok, S.; Gerhold, M. *Appl. Phys. Lett.* **2006**, *88*, 183111.
(6) Arici, E.; Sariciftci, N. S.; Meissner, D. *Adv. Funct. Mater.* **2003**, *13*, 165.
(7) Huynh, W. U.; Dittmer, J. J.; Alivisatos, A. P. *Science* **2002**, *295*, 2425.
(8) Gur, I.; Fromer, N. A.; Chen, C. P.; Kanaras, A. G.; Alivisatos, A. P. *Nano Lett.* **2007**, *7*, 409.
(9) Gowrishankar, V.; Scully, S. R.; McGehee, M. D. *Appl. Phys. Lett.* **2006**, *89*, 252102.
(10) Adikaari, A. A. D. T.; Dissanayake, D. M. N. M.; Hatton, R. A.; Silva, S. R. P. *Appl. Phys. Lett.* **2007**, *90*, 203514.
(11) Mangolini, L.; Thimsen, E.; Kortshagen, U. *Nano Lett.* **2005**, *5*, 655.
(12) Hiemenz, P. C.; Rajagopalan, R. *Principles of Colloid and Surface Chemistry*, 3rd ed.; Marcel Dekker: New York, 1997.
(13) *Static Dielectric Constants of Pure and Binary Liquid Mixtures*; Martienssen, W., Lechner, M. D., Ed.; Landolt-Börstein series, Volume 17, Supplement to IV/6; Springer: Berlin, 2008.
(14) Kim, J. S.; Granstrom, M.; Friend, R. H.; Johansson, N.; Salaneck, W. R.; Daik, R.; Feast, W. J.; Cacialli, F. *J. Appl. Phys.* **1998**, *84*, 6859.
(15) Adachi, S. *Optical Constants of Crystalline and Amorphous Semiconductors: Numerical Data and Graphical Information*; Springer: Berlin, 1999; p 29.
(16) Sensfuss, S.; Al-Ibrahim, M. In *Organic Photovoltaics: Mechanism, Materials, and Devices*; Sun, S. S., Ed.; Sariciftci, N. S., Ed.; Taylor & Francis: Boca Raton, FL, 2005; p 535.

NL8034338